

Fluorescence Imaging with One Nanometer Accuracy: Application to Molecular Motors

AHMET YILDIZ[†] AND PAUL R. SELVIN^{*,†,‡}

Center for Biophysics and Computational Biology and
Department of Physics, University of Illinois,
Urbana-Champaign, Illinois 61801

Received August 17, 2004

ABSTRACT

We introduce the technique of FIONA, fluorescence imaging with one nanometer accuracy. This is a fluorescence technique that is able to localize the position of a single dye within ~ 1 nm in the x - y plane. It is done simply by taking the point spread function of a single fluorophore excited with wide field illumination and locating the center of the fluorescent spot by a two-dimensional Gaussian fit. We motivate the development of FIONA by unraveling the walking mechanism of the molecular motors myosin V, myosin VI, and kinesin. We find that they all walk in a hand-over-hand fashion.

Introduction

Myosin V, myosin VI, and conventional kinesin are cargo-carrying motor proteins. They use energy obtained from ATP hydrolysis to transport a cargo along the cytoskeleton. Myosins move on actin, and kinesin moves on the microtubule filaments. Structurally, they all form dimers, having two motor heads held together by a common stalk. In the tail region of the stalk, they have a cargo-binding domain, which binds to specific organelles and vesicles (Figure 2). They are processive in that each motor can take hundreds of consecutive steps without detaching from the track and can move a cargo several microns. It is not clear how the two heads of a motor move to create net movement. The best approach to elucidate processive movement of the motors would be to visualize the motion of the heads as a motor walks on the cytoskeleton. However, one needs to place a nanometer-sized probe to the head region and track its position with a nanometer precision to answer such question. Here we present fluorescence imaging with one nanometer accuracy (FIONA) and its applications to motor movement.

FIONA

The image of a pointlike fluorescent object is as wide as 250 nm in the visible region of the light because of the

diffraction limit. In light microscopy, objects cannot be observed any sharper than this width. The position of an object, however, can be localized very precisely by determining the center of its emission pattern.¹ Cheezum et al. had compared different algorithms and quantitatively showed that a two-dimensional Gaussian function is the best fit to images of a single fluorescent dye, referred as a point spread function (PSF) (Figure 1A,B).² The standard error of the mean (sem) of the PSF is a measure of localization and it can be made arbitrarily small by collecting more photons and minimizing the noise factors.

An image taken by a camera contains several noise factors including photon noise, fluorescent background, camera readout, and the effect of pixelation. Thompson et al.³ had derived a theoretical calculation for the sem (σ_{μ}) as a combination of these factors and showed that all these factors can be minimized by collecting more photons:

$$\sigma_{\mu_i} = \sqrt{\left(\frac{s_i^2}{N} + \frac{a^2/12}{N} + \frac{8\pi s_i^4 b^2}{a^2 N^2} \right)}$$

where s is the standard deviation of the Gaussian distribution that equals $1/2.2$ of the PSF width, a is the pixel size, b is background and N is number of collected photons. The first term (s_i^2/N) is the photon noise, the second term is the effect of finite pixel size of the detector, and the last term is the effect of background. They also experimentally supported that the PSF center can be localized within 2 nm by using 30 nm-sized single fluorescent beads.³ Consequently, single molecules can potentially be localized with an arbitrarily high precision by increasing the signal-to-noise ratio (SNR).

Nanometer-range localization of single fluorophores on a two-dimensional surface had previously been obtained. Betzig et al.⁴ detected single lipophilic carbocyanine DiI(C₁₂) dyes frozen in PMMA matrix with a near-field scanning microscope and showed that molecules can be localized to at least $\sim \lambda/50$. Using an epifluorescence microscope, individual rhodamine dyes diffuse in a lipid bilayer⁵ and single GFP molecules in a viscous solution⁶ were tracked with ~ 30 nm precision at 5 ms. Using scanning confocal microscopy and quantum dots, Lacoste et al. resolved the distance between two nanocrystals having different emission spectra to a precision of ± 6 nm using a total integration time of 20 s.⁷ Very recently, using total internal reflection (TIRF) microscope, Dahan et al. imaged single quantum dots (15 nm in size) labeled to individual glycine receptors when they diffuse on the neuronal membrane in a living cell. They obtained ~ 5 nm localization within 75 ms integration.⁸

Organic dyes have not been bright enough to produce the amount of photons required to localize the center

Ahmet Yildiz was born in 1979 in Sakarya, Turkey. He received a B.S. in physics from the Bogazici University, Istanbul, in 2001 and started his graduate studies at University of Illinois Urbana-Champaign in the research group of Paul R. Selvin. His research focuses on single-molecule biophysics of molecular motors.

Paul R. Selvin was born in 1961 in Norwalk, Connecticut. He did his undergraduate work at the University of Michigan and graduated in 1982 with a degree in physics. He earned a physics Ph.D. from UC Berkeley in 1990 from Mel Klein initially doing EPR and later fluorescence. He did a postdoc with John Hearst in the chemistry department and continued his work on fluorescence as a staff scientist at the Lawrence Berkeley Laboratory. In 1996, he became an assistant professor at the University of Illinois at Urbana-Champaign, where he is now a full professor.

* To whom correspondence should be addressed. Mailing address: Loomis Lab of Physics, University of Illinois, 1110 W. Green St., Urbana, IL 61801. E-mail: selvin@uiuc.edu. Phone: 217-244-3371. Fax: 217-244-7559.

[†] Center for Biophysics and Computational Biology.

[‡] Department of Physics.

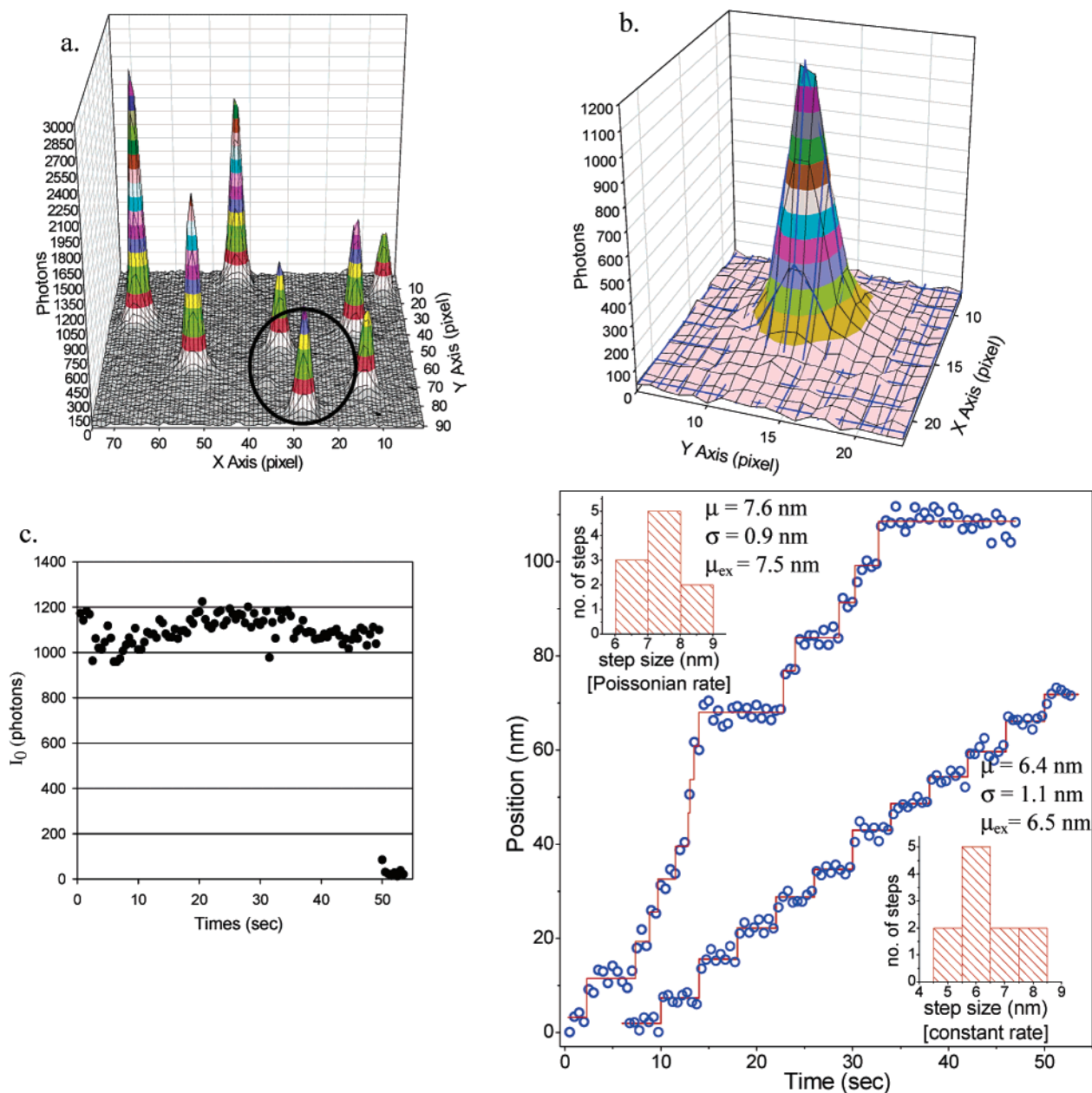


FIGURE 1. FIONA. (A) Pixelated image of several individual Cy3-dyes immobilized onto glass coverslip. Dyes were imaged by using objective-type TIR with 0.5-s integration time. (B) The PSF circled in (A) has a width of 287 nm, and the SNR of 32. A Gaussian curve-fit (solid blue line) yielded 1.3 nm precision in the center localization. (C) The dye lasted for 50 s and photobleached in a single step that indicates the image contains a single dye. (D) The PSF center versus time graph. The sample was moved with a nanometric stage with 6.5 nm increments either at a constant rate or a Poisson-distributed rate. Red lines show the average position between each step. Steps are visually separable and are determined with 1 nm precision (σ), and the accuracy [difference between the measured step size via PSF fitting (μ) and the expected step size (μ_{ex}) based on the calibrated stage] is better than 1 nm.

within one nanometer precision. They also photobleach on the order of a second, which is generally not long enough for biological applications. To extend the photostability and brightness of a single organic dye, oxygen-scavenging enzymes have been used to remove free oxygen from the solution.⁹ Oxygen collides with the molecule in its excited state and quenches the fluorescence by trapping the dye into a triplet state, which is not fluorescent. Oxygen can also undergo a chemical reaction with the dye resulting in permanent photobleaching. Addition of commonly used oxygen scavengers (glucose oxidase and catalase) can increase the photostability of a

dye roughly by 10 times. Reductants such as β -mercaptoethanol (BME) or dithiothreitol (DTT), and various salt conditions can be used to prevent the blinking of a dye and to produce a brighter signal. Previously, detection of >100,000 photons from a single molecule had been reported.^{10,11} We have optimized oxygen-scavenging and emission stabilizer conditions that led to observation of single molecules for several minutes and collection of typically 1.4 million photons before photobleaching (Figure 1C).¹²

To sensitively detect fluorescent photons, we have employed TIRF¹³ that illuminates vicinity of the glass/

water interface, resulting in minimal fluorescent background. Moreover, TIRF is a wide field technique that allows simultaneous observation of many dyes on the surface. In particular, it readily monitors full travel of many spots in motility experiments while it would be hard to track a single moving spot by using scanning confocal microscope. TIRF is also insensitive to blinking of a dye where it simply tends to decrease the overall brightness of a spot. On the contrary, blinking of a dye can yield noisier PSFs in scanning confocal microscopy since the pixels are scanned sequentially.

Objective-type TIR was the main method used since it illuminates the lower glass/water boundary that leads to slightly higher collection efficiency.¹⁴ Moreover, high N.A. oil immersion objectives can be used to obtain sharp images producing better resolution. In prism-type TIR, however, fluorescence emission passes through 100 μm of water. That may create a spherical aberration in detection and requires a water-immersion objective (N.A. = 1.2) instead of an oil objective (N.A. = 1.45–1.65) to prevent mismatch of the refractive index. To efficiently detect emitted photons and minimize the detector noise, a low-noise, back-illuminated CCD camera was used.

Figure 1A shows typical images of surface immobilized Cy3-DNA molecules acquired within 0.5 s using objective-type TIRF. The image contains approximately 14,000 photons producing SNR of 33 (Figure 1B). The emission fits perfectly well to a two-dimensional Gaussian, and yields an sem of 1.3 nm. The dye has lasted for 50 s (or 100 frames) and photobleached in a single step showing that we look at single molecules (Figure 1C). We typically collected 1.4 million photons and for some spots collected up to 5 million photons from single Cy3 dyes. One hundred consecutive images of the fluorophore were taken and the standard deviation of the position was 1.46 nm, in agreement with sem of a single image. The results also indicate that vibrations and positional drift due to thermal expansion are less than one nanometer and do not affect our results. We therefore improved spatial resolution by ~ 20 -fold and achieved sufficient precision to separate a few nanometer steps. To test this statement, artificial steps were taken by using a highly accurate (0.7 nm) piezo-electric stage. Step sizes of 6.5 nm or greater can be separated visually from each other (Figure 1D).

Positional measurements based on the PSF center are valid only if the PSF shape is symmetric. Bartko et al. showed that introducing a spherical aberration or defocusing the image can create asymmetric PSFs depending on the orientation of a dye.^{15,16} In either case, it was shown that the PSF center can change by ~ 50 nm due to the different polarization of a dye. To make sure that FIONA is not affected by the dye's orientation, we have made series of measurements. First, the Cy3 emission was unpolarized over the 0.2–0.5 s integration time—perhaps it freely rotates in this time scale. Second, bifunctional dyes on protein systems that are highly polarized on the order of 10 s (21) yielded images whose PSF is highly symmetric and well fit to a Gaussian. Third, the emission intensity of a dye labeled to a motor protein was split into

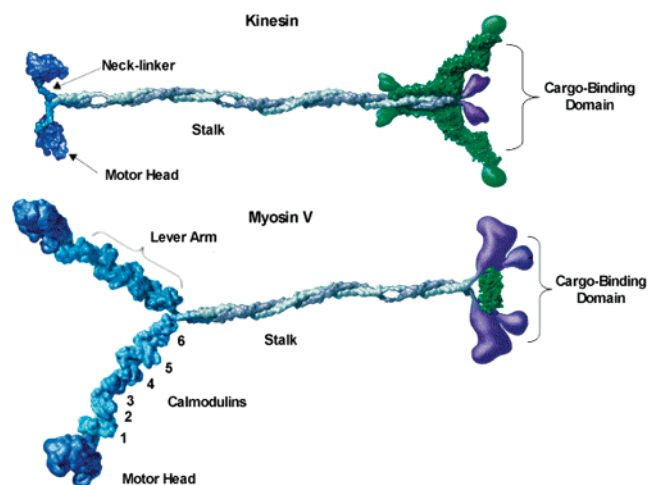


FIGURE 2. Structures of kinesin and myosin V. Conventional kinesin and myosin V form a dimer and walk processively on their track. The motor domains involved in cytoskeleton and nucleotide binding are shown in dark blue, the legs working as mechanical amplifiers are in light blue, and the stalk in purple. The stalk, formed by dimerization of alpha helical domains of monomers, connects the head regions and contains a cargo-binding domain in its tail. Other domains correspond to regulatory and cargo binding domains. Myosin VI structure looks similar to myosin V, the only exception is that it has two calmodulin-binding sites in its lever arm instead of six (see Figure 8). The figure is modified from one in ref 24.

two channels with a polarizing beam splitter. The position of a dye and the size of a step taken by a molecular motor were in total agreement between the two polarization channels. These observations clearly show that the orientational factors are not significant in our measurements.

Molecular Motors

Myosin V. Myosin V is a dimer which has the longest light-chain binding domain (24 nm), containing six calmodulin-binding sites (IQ domains) (Figure 2).^{17,18} This domain likely acts as a lever arm that amplifies small nucleotide-dependent conformational changes in the motor domain to a large displacement.^{19,20} Myosin V walks toward the plus end of actin by taking ~ 37 nm steps per ATP hydrolyzed.^{21,22} Myosin V transports a wide variety of cargo including pigment granules, membranous organelles and secretory vesicles in vertebrates, and mRNA in yeast. Functional defects in this protein cause neurological diseases and pigmentation in mice and humans.^{23–25}

Myosin VI. Myosin VI walks toward the minus end of actin filaments, in contrast to myosin V and other myosin motors.²⁶ It exists as a monomer *in vitro*,²⁷ and presumably dimerizes *in vivo* to walk processively on actin. Even though myosin VI has a very short lever arm (8 nm) relative to myosin V,²⁸ it has a 30 nm average step size—that is as large as that of myosin V.²⁹ It has a large spread in its step size that it can take 10 nm–60 nm forward steps, and 10–30 nm backward steps. Presumably, myosin VI has an elastic region which can be elongated, and takes a diffusive search during a step to create a large displacement with a significant variability.^{29,30} Studies have shown that myosin VI is involved in cell migration, spermatoge-

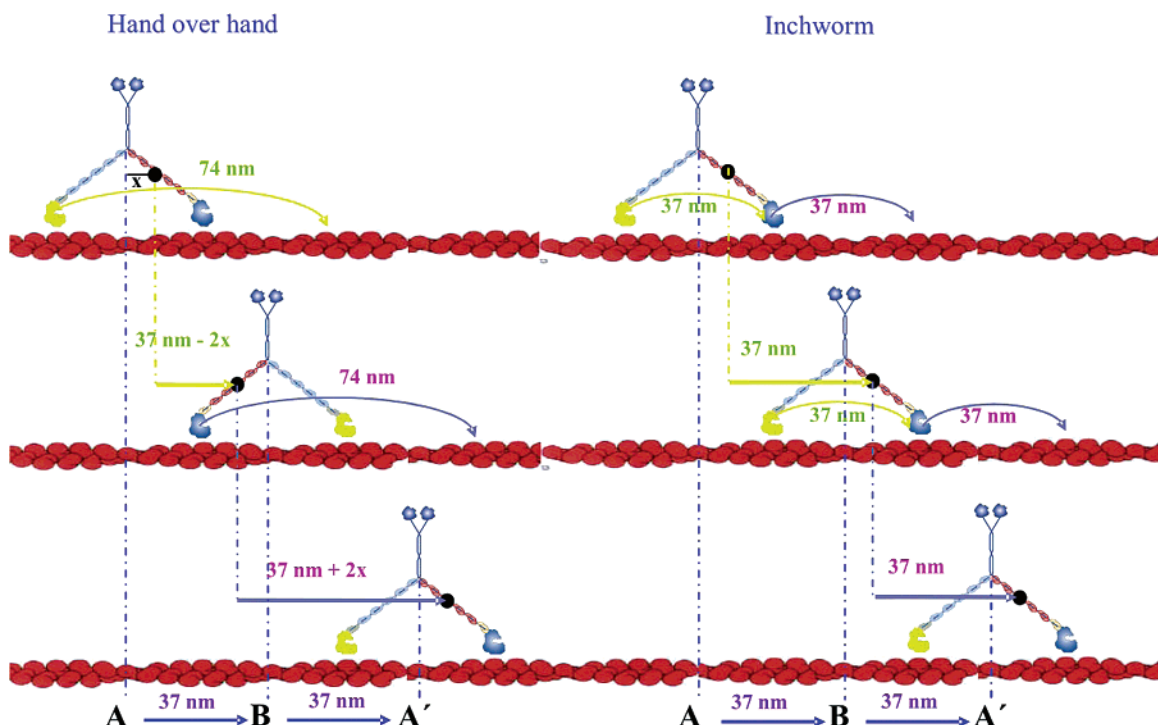


FIGURE 3. Hand-over-hand model vs Inchworm model for myosin V. In the hand-over-hand model, the rear head passes by the front head, translating a total of 74 nm, while the front head stays stationary. Therefore, heads move alternating 74 and 0 nm steps. If the dye is on the light chain, it moves $37 - 2x$, followed by $37 + 2x$ nm, where x is the distance between the dye and the center. In the inchworm model, the dye moves 37 nm regardless to where it is labeled.

nesis and signal transduction.³¹ Besides cargo transportation, myosin VI also helps positioning Golgi apparatus by anchoring it to actin cortex and stabilizes the structure of stereocilia.³² In myosin VI knockout mouse, stereocilia could not develop on the sensory hair, resulting in deafness.³³

Conventional Kinesin. Conventional kinesin (referred to simply as kinesin) is a highly processive motor that takes 8.3 nm steps along microtubules for each ATP hydrolyzed^{34–37} (Figure 1). Each head is connected to a “neck-linker”, a mechanical element that undergoes nucleotide-dependent conformational changes to enable motor stepping.³⁸ The neck linker is in-turn connected to a coiled-coil region that then leads to the cargo binding domain.³⁹ The two heads are 8 nm apart which is equal to the distance between adjacent tubulin monomers on the microtubule. It can take 100 steps/second, yielding a speed of 800 nm/sec.^{40,41} Kinesin transports a variety of cargoes, including membranous organelles, vesicles, mRNAs, intermediate filaments and signaling molecules.⁴² Mutations have been linked to neurological diseases in humans.⁴³

The Challenge

From a biophysicist perspective, the central question in understanding processive motors is to determine how the chemical and mechanical steps are coupled such that the motor moves in a coordinated manner. Processive motion of a dimeric motor suggests that one of the motor’s heads detach from the track, move forward, and attach to a next binding site. The other head must be bound to the track to prevent complete dissociation of the motor. Therefore,

active attachment/detachment of the heads must be in concert with ATP-dependent conformational changes to create a step. To explain the type of a motion, hand-over-hand model was proposed.⁴⁴ According to this model, the front head (head 1) hydrolyzes ATP, creates the power stroke, and moves the loosely attached rear head (head 2) forward. In the second step, head 2 undergoes the same cycle, while head 1 stays fixed on the track. The step size of the motor is, therefore, proportional to the length of the leg (a lever arm or a neck linker) (Figure 3).

While solution kinetics and single molecule data can be explained by a hand-over-hand mechanism, there are a number of experiments that contradicted its assumptions: 1. Nishikawa et al. observed that myosin VI heads attach to neighboring actin monomers, which never occurs in any intermediates of the hand-over-hand mechanism.⁴⁵ 2. Hua et al. performed microtubule gliding assay with conventional kinesin. At low motor concentrations they observed that single kinesin motor slides the labeled microtubule, but it does not rotate the filament. Their data implies that kinesin does not twist its stalk when it takes a step.⁴⁶ In the hand-over-hand model, a motor is expected to rotate its stalk half a revolution back and forth to revert to the same physical state after each step. That would let each head to repeat the ATPase cycle starting from the same condition. This is, however, not observed. 3. Yanagida and co-workers created a myosin V construct with a shorter lever arm and they observed that the step size does not change with a decreasing length of the lever arm.⁴⁷ (The same experiment was then repeated by using similar constructs and it was shown that the step size depends on the length of the lever arm¹⁹). 4. Observation

of a single headed processive kinesin Unc104/KIF1A implied that processivity does not always require two heads.⁴⁸ 5. Myosin VI takes long steps (30 nm average) with short legs (8 nm).²⁹

Experiments 1 and 2 resulted in a new possible mechanism called the inchworm model⁴⁹ where only one head catalyzes ATP and always leads while the other head follows (Figure 3). After each step, the motor can turn back to the exact same state without rotating its stalk. However, this model vaguely suggests that two conformational changes occur for a single ATP hydrolysis because both of the heads move forward during a step. Results of 3, 4 and 5 show that step size is not relevant to the length of the motor leg and the motor does not require two heads to move processively. To explain these data, biased diffusion of a motor along actin/microtubule lattice was proposed.⁴⁷ In this mechanism, once a motor detaches from the cytoskeleton, it diffuses along the track and binds to another actin/tubulin monomer along the forward direction. The bias is given by an initial push created by the powerstroke. However, this model cannot directly explain how the motor can reattach to the track when it is fully detached and how the step mediated by diffusion has a well-defined value.

The most direct way to distinguish between these models is to measure how much each head moves while the motor walks. The hand-over-hand model states that a head alternately moves twice the stalk displacement and stays stationary while the other head takes a step. For example, if a person moves 30 cm with each step, each foot would take 60 cm, 0 cm, 60 cm, 0 cm alternating steps. The inchworm model (Figure 3) predicts that each head moves forward as much as the stalk. If a person would walk with an inchworm mechanism, when the body moves 30 cm forward, both of the feet would move 30 cm forward, too.

Current nanometer tracking techniques, optical trap and cantilever probe microscopy, are not readily applicable to track the head movement. This is because they use a probe that is much bigger than motor's tiny heads, implying that attachment of the bead to the head region would sterically hinder the motion. FIONA uses a nanometer sized organic dye and provides sufficient spatial resolution to separate 8 nm versus 16 nm steps taken by a kinesin head, and 36 nm versus 72 nm taken by myosin V and myosin VI heads. The time resolution of FIONA (300 ms) is not adequate to detect the individual steps of the motor in cellular conditions, which is roughly 10 ms per step. Fortunately, motors can be slowed in vitro by using a low amount of ATP so that they take one step per second. To determine how the motors walk, we have labeled a single head of a dimeric motor with a single dye and performed a FIONA assay.

Application to Processive Motors

Myosin V. We labeled calmodulin with a single bifunctional rhodamine (BR) and exchanged it into chick-brain myosin V.^{12,20} The calmodulin can potentially exchange anywhere on the myosin V light chain. The inchworm

model predicts a uniform step size of 37 nm, regardless of which IQ domain is exchanged with a labeled calmodulin. On the other hand, the hand-over-hand model predicts alternating short and long steps of $37 - 2x$, $37 + 2x$, where x is the in-plane distance of the dye from the midpoint of the myosin (Figure 3).¹²

In the FIONA assay, the labeled myosin V motors on actin filaments can be located within ± 3 nm typically, and ± 1.5 nm for brighter spots. Almost all of the spots showed single step photobleaching, indicative of single molecules and only those spots were analyzed in further experiments. By addition of 300 nM ATP, most of the spots moved an average of 6 nm/sec. We observed three classes of steps. The vast majority of molecules displayed uniform 74 nm displacements in agreement with the hand-over-hand mechanism (Figure 4). The labeled calmodulin yielding this stepping pattern was most likely exchanged on the first IQ domain. Alternating short and long steps were also observed arising from exchanging labeled calmodulins to other IQ domains (Figure 5). From the $37 - 2x$, $37 + 2x$ assumption, 52–23 nm alternating steps belong to molecules labeled at the fifth IQ domain, where 42–33 nm steps belonged to the sixth IQ domain.¹²

Each 74 nm step should alternate with a 0 nm step in the hand-over-hand model. While 0 nm steps cannot be detected directly from the position, a kinetic analysis revealed that 74 nm traces are significantly different from 52 to 23 nm and 42–33 nm traces. This is because 74 nm displacements are the convolution of two distinct steps (74 and 0 nm) whereas each individual steps (i.e., 42 and 33 nm steps) can be directly seen in the other two classes of traces. It should be noted that, each step taken by myosin V is limited by ATP binding at our conditions (340 nM ATP). This is expected to yield an exponential decay where each step can be observed. The results showed that the dwell time histogram of 52–23 nm and 42–33 nm traces displayed exponential decay while those of 74 nm traces fit well to a convolution function (Figure 6).¹²

It is a bit surprising that a dye on the light-chain displays 74–0 nm. Strictly speaking, only a dye on the head should display such behavior. One possibility is that this zero nanometer step is not quite zero such that we cannot resolve this small amount. Another possibility is that the myosin V lever arm is not a rigid rod, instead, the front lever arm is bent toward the direction of motion. Such a configuration, named a telemark skier, was observed in cryoEM images of actomyosinV. We also measured the motion of the myosin V head by labeling an eGFP to the N terminus of the head. It also revealed the same 74–0 nm stepping pattern, in agreement with the telemark skier configuration of myosin V on actin.⁵⁰

Kinesin. A “Cys-light” human ubiquitous kinesin with all solvent-exposed cysteines replaced, was used as a template. A single cysteine was replaced at different positions on the head region and those cysteines were labeled with a single Cy3 molecule. Labeled motors were introduced into the flow chamber after immobilizing *axonemes* on the glass surface. (Axoneme is a microtubule rich structure that is more rigid than microtubules,

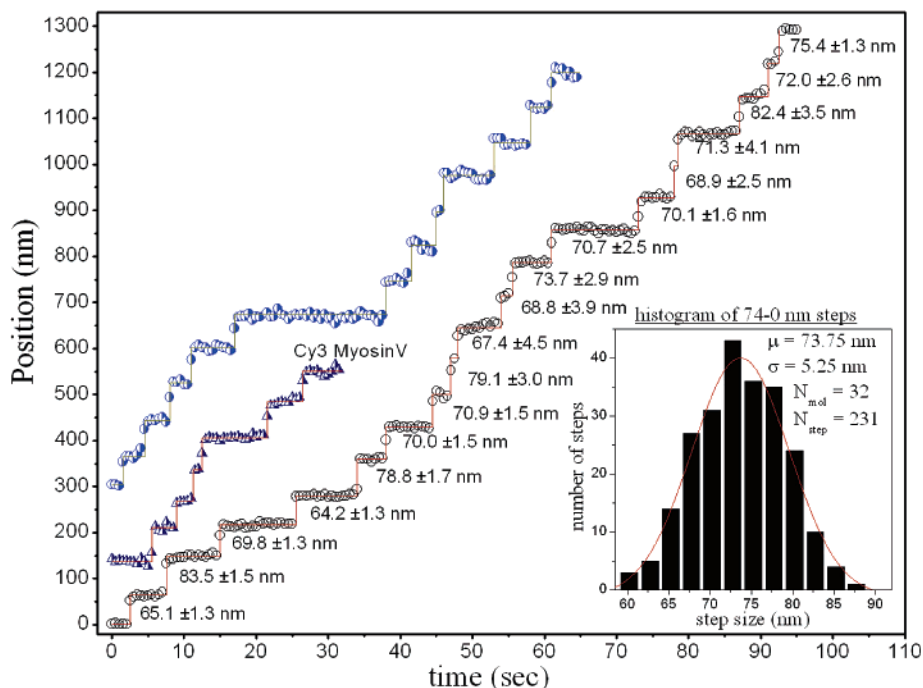


FIGURE 4. Stepping traces of three different myosin V molecules displaying 74 nm steps, and histogram of a total of 32 myosin V's taking 231 steps. Traces are for BR-labeled myosin V unless noted as Cy3.

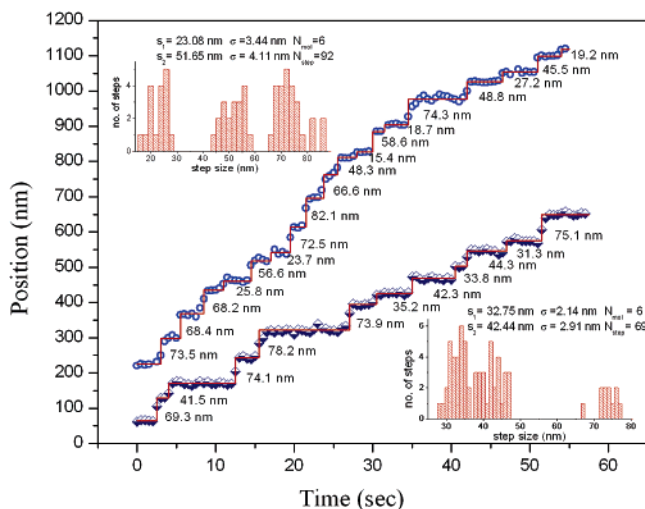


FIGURE 5. Stepping traces of two different BR-labeled myosin V molecules displaying alternating 52–23 nm and 42–33 nm steps according to position of the dye on the motor. Cumulative step size histogram of six myosin V's showing 52–23 nm steps (left above insert) and seven myosin V's showing 42–33 nm steps (right below insert) displays three distinct peaks. First two peaks from left correspond to alternating short and long steps. The third peak is the sum of two steps (short + long) since some steps are missed and yield 74 nm apparent steps due to the 0.5 s time resolution of measurements.

providing better surface immobilization.) At 340 nM ATP, the spots moved an average of 8.3 nm/sec (Figure 7A). What we observed is that the head takes 17.3 ± 3.3 nm steps, strongly supportive of the hand-over-hand mechanism (Figure 7C). 8.3 nm steps were not observed, excluding the inchworm model. Kinetic analysis of dwell times revealed that 17 nm steps alternate with 0 nm steps showing that the head moves twice the stalk movement

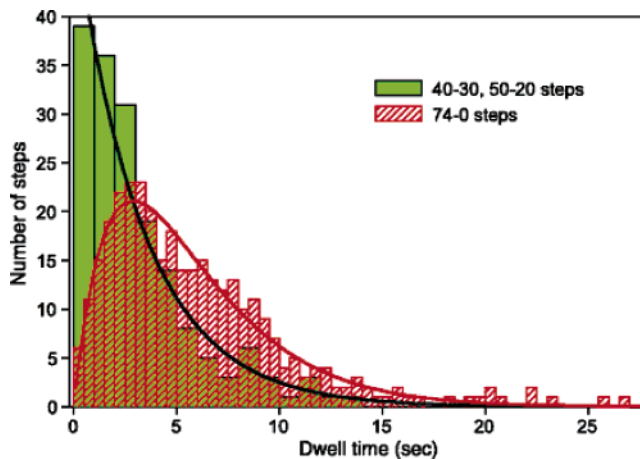


FIGURE 6. The dwell time histograms for 74–0 nm steps (red crosshatched) displays an initial rise and then decays slowly. The distribution fits well to a convolution of two steps. This indicates that each dwell period between 74 nm steps corresponds to two steps of myosin V. This further shows the head takes twice the center-of-mass step size (74 nm displacement), and then stays bound to actin (no displacement), while the other head moves forward, supportive of a hand-over-hand mechanism. As a proof of this concept, the dwell-time histogram of 40–30 and 50–20 nm steps (solid green) decays exponentially. The data indicates that every dwell period correspond to a single step of myosin V.

and stays bound to microtubule in the second step while the other (unlabeled) head moves forward (Figure 7C).⁵¹

Myosin VI. We have labeled myosin VI either with an eGFP on its motor domain or with a single Cy3 on a calmodulin binding site (Figure 8A). To place a fluorophore on the motor domain, an eGFP-myosin VI fusion protein was created with an eGFP at the N-terminus of the motor. Labeled calmodulins exchange only with the second binding site on the lever arm.⁵² The myosin VI

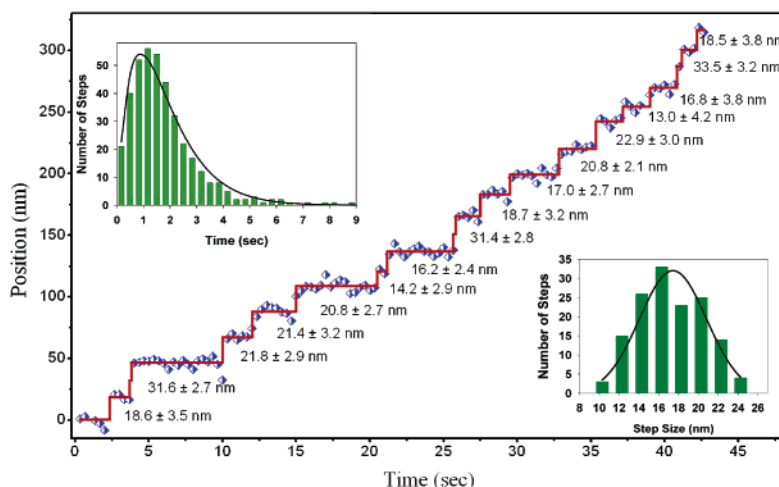


FIGURE 7. Stepping pattern of an individual head of kinesin. The blue dots with solid red lines correspond to the motion of the single head of kinesin walking on an immobilized microtubule. The head takes a step that is twice the stalk movement (16.6 nm) showing that kinesin uses a hand-over-hand mechanism. The average step size is 17.3 ± 3.3 nm (right insert). 16.6 nm (and its multiples) were observed due to finite time resolution. 8.3 nm and its odd multiples were not observed which excludes the inchworm type of walking. The kinetic analysis of the dwell time histogram (left insert) is a convolution of two steps of kinesin, showing that kinesin's heads indeed alternate 16.6 nm, 0 nm steps.⁵¹

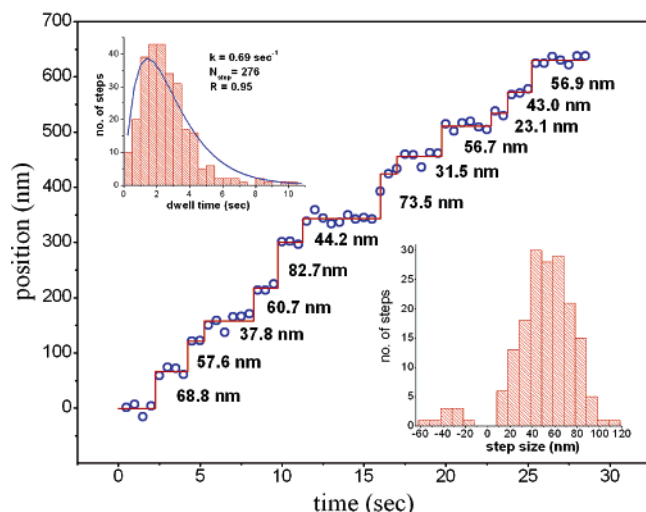
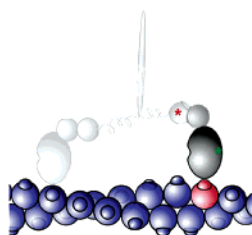


FIGURE 8. Myosin VI. (A) The myosin was labeled either on the head with eGFP, or on the second light chain with calmodulin. (B) Stepping trace of Cy3-labeled myosin VI molecule display an average of ~ 60 nm steps. The step size histogram (inset below, right) of a total of 33 myosin VI's taking 176 steps. The data shows that myosin VI walks hand over hand, like kinesin and myosin V. The average forward step size measured is 55.2 ± 19.6 nm ($N = 167$) and backward step size is -31.7 ± 8.6 nm as expected based upon optical trap measurements. Dwell time histogram fits well to a convolution function showing that the head moves by alternating 60–0 nm steps (upper right).⁵²

heavy chain was truncated after the coiled-coil domain and a leucine zipper was added to stabilize dimerization. In the FIONA assay, 10–40 μM ATP was used to get

appropriate stepping rate (~ 0.5 – 1 step/sec) for myosin VI. We found that the head region takes approximately 60 nm steps⁵² (Figure 8B). Motors labeled with either an eGFP to the head or Cy3 to the light chain gave the same result and clearly supported a hand-over-hand mechanism. The distribution of the step size histogram agrees with the published optical trap data (Figure 8B and ref 29). Both of the eGFP- and Cy3- histograms show that steps of myosin VI have a very broad distribution and the motor takes forward and backward steps. Kinetic analysis again highlights the presence of 0 nm hidden steps, giving an additional support to hand-over-hand motion (Figure 8B).⁵² Unexpectedly, Cy3-calmodulin showed significant fluctuation in its ATP state while it is highly immobile in the rigor and ADP state. This implies that in some part of myosin VI's ATP state, the lever arm uncouples from the motor, which may potentially arise from the proposed elongation of the lever arm.

Conclusion

We established a new technique that provides localization of surface immobilized single organic dyes with better than 1.5 nm precision. The way to achieve a nanometer precision is collecting more photons and minimizing the background. We applied FIONA to the molecular motors myosin V, kinesin, and myosin VI, to understand how they walk processively along the cytoskeleton. A single organic dye was either labeled on the head region, or on the lever arm, and its motion was tracked as the motor moves on its respective track, in vitro. What we have found is that these motors move by swapping their rear head forward while the front head stays bound to the track, called hand-over-hand. We excluded an inchworm model where one head leads and the other head follows.

Several groups have also presented strong evidence for a hand-over-hand walking for kinesin,^{53,54} myosin V,²⁰ and myosin VI.⁵⁵ The next challenge will be to find out whether

they walk symmetrically or asymmetrically. The symmetric model proposes that the motor reverts to the same physical structure that requires a motor to rotate its coiled-coil stalk half a revolution back and forth every step. Alternately, the asymmetric model avoids the rotation of the stalk and proposes that the motor alternates between two distinct physical states. Therefore, the two heads would follow different stepping pathways. That would cause a motor to take alternating fast and slow steps when ATP concentration is saturating. Such limping was observed for truncated constructs of kinesin and mutant homodimeric kinesins but was not observed for the wild-type.^{54,56} Presenting direct evidence to the question of whether the stalk rotates would be critical to understand how processive motors function in a cell. We anticipate FIONA will be able to distinguish between symmetric versus asymmetric models by directly observing motor protein's motion.

Future Directions

Two-Color FIONA. FIONA is currently a one-color technique that provides nanometer precision tracking of a single position on a biological entity. Potentially, two different dyes can simultaneously be tracked by separating fluorescence to two channels on a camera. Two-color FIONA can be used to measure the translational motion and the absolute distances of two specific sites.

Using Quantum Dots in FIONA. Temporal resolution of FIONA is currently on the order of 100 ms that is somewhat low for cellular processes. Performing an experiment under physiological conditions will require a higher fluorescence signal. Quantum dots are twenty times brighter than organic dyes and provide much longer photostability. This implies that we can obtain nanometer precision with twenty times faster rate, and track a molecule much longer than organic dyes. In preliminary experiments using surface immobilized quantum dots, 8 nm steps created by piezo-electric stage with a stepping rate of 10 Hz were easily separated. This is 10-fold improvement in our time resolution and it can be further increased to perform single molecule experiments *in vivo*, and/or at saturating ATP levels.

In Vivo FIONA Assay. Technically, it is not easy to achieve single molecule sensitivity within a cell because cytoplasm creates high levels of autofluorescence, which exceeds signal levels of an organic dye. However, using quantum dots can also extend the application of FIONA to *in vivo* assays because they can potentially be detected with a high SNR. We have recently used extremely bright GFP-containing peroxisomes to watch them move *in vivo* with 1 ms temporal resolution and 1.5 nm spatial resolution.⁵⁷ *In vivo* FIONA assay can be used to understand how the cargoes are transported back and forth within a cell.

FIONA has renovated the single molecule field and provided unequivocal answers for the ongoing debates in biophysics. The potential applications extending to newer directions are yet to come.

This work was supported by NIH and NSF.

References

- (1) Bevington, P. R.; Robinson, D. K. *Data Reduction and Error Analysis for the Physical Sciences*, 3rd ed.; McGraw-Hill: Indianapolis, IN, 2002.
- (2) Cheezum, M. K.; Walker, W. F.; Guilford, W. H. Quantitative comparison of algorithms for tracking single fluorescent particles. *Biophys. J.* **2001**, *81* (4), 2378–2388.
- (3) Thompson, R. E.; Larson, D. R.; Webb, W. W. Precise nanometer localization analysis for individual fluorescent probes. *Biophys. J.* **2002**, *82* (5), 2775–2783.
- (4) Betzig, E.; Chichester, R. J. Single Molecules Observed By Near-Field Scanning Optical Microscopy. *Science* **1993**, *262* (5138), 1422–1425.
- (5) Schmidt, T.; Schutz, G. J.; Baumgartner, W.; Gruber, H. J.; Schindler, H. Imaging of Single Molecule Diffusion. *Proc. Natl. Acad. Sci. U.S.A.* **1996**, *93* (7), 2926–2929.
- (6) Kubitschek, U.; Kuckmann, O.; Kues, T.; Peters, R. Imaging and tracking of single GFP molecules in solution. *Biophys. J.* **2000**, *78* (4), 2170–2179.
- (7) Lacoste, T. D.; Michalet, X.; Pinaud, F.; Chemla, D. S.; Alivisatos, A. P.; Weiss, S. Ultrahigh-resolution multicolor colocalization of single fluorescent probes. *Proc. Natl. Acad. Sci. U.S.A.* **2000**, *97* (17), 9461–9466.
- (8) Dahan, M.; Levi, S.; Luccardini, C.; Rostaing, P.; Riveau, B.; Triller, A. Diffusion dynamics of glycine receptors revealed by single-quantum dot tracking. *Science* **2003**, *302* (5644), 442–445.
- (9) Harada, Y.; Sakurada, K.; Aoki, T.; Thomas, D. D.; Yanagida, T. Mechanochemical coupling in actomyosin energy transduction studied by *in vitro* movement assay. *J. Mol. Biol.* **1990**, *216* (1), 49–68.
- (10) Adachi, K.; Yasuda, R.; Noji, H.; Itoh, H.; Harada, Y.; Yoshida, M.; Kinoshita, K., Jr. Stepping rotation of F1-ATPase visualized through angle-resolved single-fluorophore imaging. *Proc. Natl. Acad. Sci. U.S.A.* **2000**, *97* (13), 7243–7247.
- (11) Sambongi, Y.; Iko, Y.; Tanabe, M.; Omote, H.; Iwamoto-Kihara, A.; Ueda, I.; Yanagida, T.; Wada, Y.; Futai, M. Mechanical Rotation of the c Subunit Oligomer in ATP Synthase (F0F1): Direct Observation. *Science* **1999**, *286*, 1722–1724.
- (12) Yildiz, A.; Forkey, J. N.; McKinney, S. A.; Ha, T.; Goldman, Y. E.; Selvin, P. R. Myosin V walks hand-over-hand: single fluorophore imaging with 1.5-nm localization. *Science* **2003**, *300* (5628), 2061–2065.
- (13) Axelrod, D. Total internal reflection fluorescence microscopy. *Methods Cell Biol.* **1989**, *30*, 245–270.
- (14) Tokunaga, M.; Kitamura, K.; Saito, K.; Iwane, A. H.; Yanagida, T. Single Molecule Imaging of Fluorophores and Enzymatic Reactions Achieved By Objective-Type Total Internal Reflection Fluorescence Microscopy. *Biochem. Biophys. Res. Commun.* **1997**, *235* (1), 47–53.
- (15) Bartko, A. P.; Dickson, R. M. Three-Dimensional Orientations of Polymer-Bound Single Molecules. *J. Phys. Chem. B* **1999**, *103* (16), 3053–3056.
- (16) Bartko, A. P.; Dickson, R. M. Imaging Three-Dimensional Single Molecule Orientations. *J. Phys. Chem. B* **1999**, *103* (51), 11237–11241.
- (17) Espindola, F. S.; Suter, D. M.; Partata, L. B.; Cao, T.; Wolenski, J. S.; Cheney, R. E.; King, S. M.; Mooseker, M. S. The light chain composition of chicken brain myosin-Va: calmodulin, myosin-II essential light chains, and 8-kDa dynein light chain/PIN. *Cell Motil. Cytoskeleton* **2000**, *47* (4), 269–281.
- (18) Cheney, R. E.; O'Shea, M. K.; Heuser, J. E.; Coelho, M. V.; Wolenski, J. S.; Espreafico, E. M.; Forscher, P.; Larson, R. E.; Mooseker, M. S. Brain myosin-V is a two-headed unconventional myosin with motor activity. *Cell* **1993**, *75* (1), 13–23.
- (19) Purcell, T. J.; Morris, C.; Spudich, J. A.; Sweeney, H. L. Role of the lever arm in the processive stepping of myosin V. *Proc. Natl. Acad. Sci. U.S.A.* **2002**, *99* (22), 14159–14164.
- (20) Forkey, J. N.; Quinlan, M. E.; Shaw, M. A.; Corrie, J. E.; Goldman, Y. E. Three-dimensional structural dynamics of myosin V by single-molecule fluorescence polarization. *Nature* **2003**, *422* (6930), 399–404.
- (21) Mehta, A. D.; Rock, R. S.; Rief, M.; Spudich, J. A.; Mooseker, M. S.; Cheney, R. E. Myosin-V is a processive actin-based motor. *Nature* **1999**, *400* (6744), 590–593.
- (22) Veigel, C.; Wang, F.; Bartoo, M. L.; Sellers, J. R.; Molloy, J. E. The gated gait of the processive molecular motor, myosin V. *Nat. Cell Biol.* **2002**, *4* (1), 59–65.
- (23) Reck-Peterson, S. L.; Provance, D. W., Jr.; Mooseker, M. S.; Mercer, J. A. Class V myosins. *Biochim. Biophys. Acta* **2000**, *1496* (1), 36–51.
- (24) Vale, R. D. The molecular motor toolbox for intracellular transport. *Cell* **2003**, *112* (4), 467–480.

- (25) Vale, R. D. Myosin V motor proteins: marching stepwise towards a mechanism. *J. Cell Biol.* **2003**, *163* (3), 445–450.
- (26) Wells, A. L.; Lin, A. W.; Chen, L. Q.; Safer, D.; Cain, S. M.; Hasson, T.; Carragher, B. O.; Milligan, R. A.; Sweeney, H. L. Myosin VI is an actin-based motor that moves backwards. *Nature* **1999**, *401* (6752), 505–508.
- (27) Lister, I.; Schmitz, S.; Walker, M.; Trinick, J.; Buss, F.; Veigel, C.; Kendrick-Jones, J. A monomeric myosin VI with a large working stroke. *EMBO J.* **2004**, *23* (8), 1729–1738.
- (28) Bahloul, A.; Chevreux, G.; Wells, A. L.; Martin, D.; Nolt, J.; Yang, Z.; Chen, L. Q.; Potier, N.; Van Dorsselaer, A.; Rosenfeld, S.; Houdusse, A.; Sweeney, H. L. The unique insert in myosin VI is a structural calcium-calmodulin binding site. *Proc. Natl. Acad. Sci. U.S.A.* **2004**, *101* (14), 4787–4792.
- (29) Rock, R. S.; Rice, S. E.; Wells, A. L.; Purcell, T. J.; Spudich, J. A.; Sweeney, H. L. Myosin VI is a processive motor with a large step size. *Proc. Natl. Acad. Sci. U.S.A.* **2001**, *98* (24), 13655–13659.
- (30) Altman, D.; Sweeney, H. L.; Spudich, J. A. The mechanism of myosin VI translocation and its load-induced anchoring. *Cell* **2004**, *116* (5), 737–749.
- (31) Cramer, L. P. Myosin VI: roles for a minus end-directed actin motor in cells. *J. Cell Biol.* **2000**, *150* (6), F121–F126.
- (32) Buss, F.; Luzio, J. P.; Kendrick-Jones, J. Myosin VI, an actin motor for membrane traffic and cell migration. *Traffic* **2002**, *3* (12), 851–858.
- (33) Avraham, K. B.; Hasson, T.; Steel, K. P.; Kingsley, D. M.; Russell, L. B.; Mooseker, M. S.; Copeland, N. G.; Jenkins, N. A. The mouse Snell's waltzer deafness gene encodes an unconventional myosin required for structural integrity of inner ear hair cells. *Nat. Genet.* **1995**, *11* (4), 369–375.
- (34) Svoboda, K.; Schmidt, C. F.; Schnapp, B. J.; Block, S. M. Direct observation of kinesin stepping by optical trapping interferometry. *Nature* **1993**, *365* (6448), 721–727.
- (35) Howard, J.; Hudspeth, A. J.; Vale, R. D. Movement of microtubules by single kinesin molecules. *Nature* **1989**, *342* (6246), 154–158.
- (36) Vale, R. D.; Milligan, R. A. The way things move: looking under the hood of molecular motor proteins. *Science* **2000**, *288* (5463), 88–95.
- (37) Kozielski, F.; Sack, S.; Marx, A.; Thormahlen, M.; Schonbrunn, E.; Biou, V.; Thompson, A.; Mandelkow, E. M.; Mandelkow, E. The crystal structure of dimeric kinesin and implications for microtubule-dependent motility. *Cell* **1997**, *91* (7), 985–994.
- (38) Rice, S.; Lin, A. W.; Safer, D.; Hart, C. L.; Naber, N.; Carragher, B. O.; Cain, S. M.; Pechatnikova, E.; Wilson-Kubalek, E. M.; Whittaker, M.; Pate, E.; Cooke, R.; Taylor, E. W.; Milligan, R. A.; Vale, R. D., A structural change in the kinesin motor protein that drives motility. *Nature* **1999**, *402* (6763), 778–784.
- (39) Vale, R. D.; Fletterick, R. J. The design plan of kinesin motors. *Annu. Rev. Cell. Dev. Biol.* **1997**, *13*, 745–77.
- (40) Coy, D. L.; Wagenbach, M.; Howard, J. Kinesin takes one 8-nm step for each ATP that it hydrolyzes. *J. Biol. Chem.* **1999**, *274* (6), 3667–3671.
- (41) Vale, R. D.; Funatsu, T.; Pierce, D. W.; Romberg, L.; Harada, Y.; Yanagida, T. Direct observation of single kinesin molecules moving along microtubules. *Nature* **1996**, *380* (6573), 451–453.
- (42) Goldstein, L. S.; Philp, A. V. The road less traveled: emerging principles of kinesin motor utilization. *Annu. Rev. Cell. Dev. Biol.* **1999**, *15*, 141–183.
- (43) Reid, E.; Kloos, M.; Ashley-Koch, A.; Hughes, L.; Bevan, S.; Svenson, I. K.; Graham, F. L.; Gaskell, P. C.; Dearlove, A.; Pericak-Vance, M. A.; Rubinsztein, D. C.; Marchuk, D. A. A kinesin heavy chain (KIF5A) mutation in hereditary spastic paraplegia (SPG10). *Am. J. Hum. Genet.* **2002**, *71* (5), 1189–1194.
- (44) Spudich, J. A. The myosin swinging cross-bridge model. *Nat. Rev. Mol. Cell. Biol.* **2001**, *2* (5), 387–392.
- (45) Nishikawa, S.; Homma, K.; Komori, Y.; Iwaki, M.; Wazawa, T.; Hikikoshi Iwane, A.; Saito, J.; Ikebe, R.; Katayama, E.; Yanagida, T.; Ikebe, M. Class VI myosin moves processively along actin filaments backward with large steps. *Biochem. Biophys. Res. Commun.* **2002**, *290* (1), 311–317.
- (46) Hua, W.; Chung, J.; Gelles, J. Distinguishing inchworm and hand-over-hand processive kinesin movement by neck rotation measurements. *Science* **2002**, *295* (5556), 844–848.
- (47) Tanaka, H.; Homma, K.; Iwane, A. H.; Katayama, E.; Ikebe, R.; Saito, J.; Yanagida, T.; Ikebe, M. The motor domain determines the large step of myosin-V. *Nature* **2002**, *415* (6868), 192–195.
- (48) Okada, Y.; Higuchi, H.; Hirokawa, N. Processivity of the single-headed kinesin KIF1A through biased binding to tubulin. *Nature* **2003**, *424* (6948), 574–577.
- (49) Hua, W.; Young, E. C.; Fleming, M. L.; Gelles, J. Coupling of kinesin steps to ATP hydrolysis. *Nature* **1997**, *388* (6640), 390–393.
- (50) Snyder, G. E.; Sakamoto, T.; Hammer, J. A., 3rd; Sellers, J. R.; Selvin, P. R. Nanometer localization of single green fluorescent proteins: evidence that myosin V walks hand-over-hand via telemark configuration. *Biophys. J.* **2004**, *87* (3), 1776–1783.
- (51) Yildiz, A.; Tomishige, M.; Vale, R. D.; Selvin, P. R. Kinesin Walks Hand-Over-Hand. *Science* **2004**, *303*, 676–678.
- (52) Yildiz, A.; Park, H.; Safer, D.; Yang, Z.; Chen, L. Q.; Selvin, P. R.; Sweeney, H. L. Myosin VI Steps via a Hand-over-Hand Mechanism with Its Lever Arm Undergoing Fluctuations when Attached to Actin. *J. Biol. Chem.* **2004**, *279* (36), 37223–37226.
- (53) Kaseda, K.; Higuchi, H.; Hirose, K. Alternate fast and slow stepping of a heterodimeric kinesin molecule. *Nat. Cell Biol.* **2003**, *5* (12), 1079–1082.
- (54) Asbury, C. L.; Fehr, A. N.; Block, S. M. Kinesin moves by an asymmetric hand-over-hand mechanism. *Science* **2003**, *302* (5653), 2130–2134.
- (55) Okten, Z.; Churchman, L. S.; Rock, R. S.; Spudich, J. A. Myosin VI walks hand-over-hand along actin. *Nat. Struct. Mol. Biol.* **2004**, *11* (9), 884–887.
- (56) Higuchi, H.; Bronner, C. E.; Park, H. W.; Endow, S. A. Rapid double 8-nm steps by a kinesin mutant. *EMBO J.* **2004**, *23* (15), 2993–2999.
- (57) Kural, C.; Kim, H.; Syed, S.; Goshima, G.; Gelfand, V. I.; Selvin, P. R. Kinesin and Dynein Moving a GFP-labeled Peroxisome In Vivo: A Tug-of-War or Coordinated Movement? *Science*, submitted for publication.

AR040136S